Simulation of Heat Flow in Aluminum Sand Casting

El Hassan E. M. Khalafalla & Hashim A. A. El Hashimi *

ملخص

تهتم هذه الورقة بدراسة انسياب الحرارة فى مسبوك المونيوم شكل .T فى قالب رملى لاجل تقليص نطاق عملية التصميم حتى تتكامل آنياً مع اعمال المسبك.

تم اجراء تحليل عددى لاخطى لانتقال الحرارة العابرة فى بعدين أثناء الدورة الكاملة لشريحة المصبوبة بسمك الوحدة ، بإستخدام طريقة الفروق المحدودة و برنامج ماتلاب الاصدارة 6.1 .

نسبة لقلة المعلومات فيما يتعلق بالعملية الحقيقية للسباكة فى المسبك، فلقد تم اجراء المحاكاة العددية على النموذج باستخدام خواص فيزيائية ثابتة للمواد، ومجموعات مبسطة للأحوال الابتدائية والحدودية . تم افتراض توزيع منتظم لدرجات الحرارة الابتدائية فى السبيكة والقالب لحالة مسبوكة صبت تلقائياً فى القالب. وفقاً للتماثل المحورى، فقط تمت محاكاة النصف الأيمن للنموذج لأجل تقليل التحليل. أهملت آثار الأشعاع الحرارى وسمك الجدران الخارجية لصندوقى القالب على العملية.

* Department of Production Engineering, Faculty of Eng. & Tech.
Nile Valley University

Abstract

This paper deals with the study of heat flow in a T-shaped aluminum casting in sand mould, in order to contract the design process envelope to be integrated with foundry practices concurrently.

A two-dimensional non-linear numerical analysis of transient heat transfer during the complete cycle of unit thick slice of casting was performed using the finite differences method and the MATLAB Rel.6.1 package.

The numerical simulation was carried out on model and constant physical material properties, simplified sets of boundary and initial conditions, were introduced in the model due to the lack of information regarding the real casting process in foundry. Uniform initial temperatures distribution in sand and alloy were assumed, for case of casting already infused in the mould. Due to axisymmetry, only the right half of the model was simulated to reduce analysis. The effect of thermal radiation and thickness of outer boxes of mould on the process were neglected.

The results of temperature, cooling rate and temperature gradient distributions in the aluminum casting and mould during the

solidification process were shows that the geometry of the section influence the regions at which solidification starts and ends. Meanwhile the heat flow-related properties shows that, the last solidified regions could be the most probable locations of defects. The results obtained show concrete agreement with the previous works, that reflected the defects criteria and demonstrated the behaviour of the system logically.

Keywords: casting, finite element method, Simulation, nonlinear transient thermal analysis, defects.

1- Introduction

The metal casting process is the simplest, most direct route to a near net shape product, and often the least expensive. This process in its fundamental form requires a mould cavity of the desired shape and molten metal to pour into the mould cavity [1]. The production of molten metal and mould to make castings has traditionally been an art form, an expression of human creativity carried out both for aesthetic and practical reasons. The computer simulation of casting process has emerged as a powerful tool for achieving quality assurance without time consuming trails. Simulating the solidification of molten metal in the mould

enables predicting the location of shrinkage defect and optimizing the design of feeders to improve the yield. It has been reported that simulation studies can reduce by as much as 25% the casting defects, manufacturing costs and lead time [2]. Simulation of heat flow in casting process enables visualization of the progress of freezing inside a casting during the solidification phase and identification of the last freezing regions or hot spots. This facilitates the placement of and design of feeders and feeding aids in order to maximize yield while ensuring casting soundness without expensive and time-consuming trails runs. It is also a valuable tool for product designers as it allows the solidification of a casting to be considered during the design phase [3].

The feeder design can be verified by casting trials to find the location and distribution of shrinkage porosity. Besides being expensive and time-consuming, shop floor trials may not provide a complete and correct picture, leading to unexpected defects during regular production. This can be overcome by virtual casting trials using simulation software for defect prediction and yield optimization[4].

Numerical methods for solidification simulation have received considerable attention from researchers in the past three decades [5]. The casting shape is broken down into a number of simple elements and the heat conduction equation is applied to them over a number of time steps in order to obtain the temperatures at different nodes. Finite difference (FDM), finite element (FEM) and recently geometric methods such as boundary element (BEM); modulus vector (MVM) have been used[6].

Numerical simulation of the casting process has gradually moved from research to practical application in the last few years. Several packages based on either FDM or FEM are currently available and being used in the industry. A typical iteration involves solid modeling, mesh generation, material selection, specification of boundary conditions, numerical computations and finally post-processing for viewing the results (usually plotting of colour coded temperature at different time steps and displaying macro-and micro shrinkage cavities)[7].

The problem of heat flow in the model is simplified assuming that alloy is already infused into sand mould. This non-linear transient thermal analysis problem is numerically solved using

finite elements coupled with finite differences methods. Conduction occurs between the alloy and the sand mould, and convection occurs between the sand mould and the ambient air. It was supposed that solidification process starts at temperature level of 640°C and finishes at 620°C and that the latent heat of solidification releases in this range. Because of small cross section and weight of inner and outer box of casting, we neglected their influence on the process. Radiation phenomena are also neglected.

2- Mathematical Model

In heat transfer problems, the governing equations represent the balance of mass, momentum, and energy for a medium. Applying the principle of the conservation of energy to a system represented in a Cartesian coordinate system results in the following transient two-dimensional heat diffusion equation:

$$K_x \frac{\partial^2 T}{\partial x^2} + K_y \frac{\partial^2 T}{\partial y^2} + \dot{q} = C\rho \frac{\partial T}{\partial t} \qquad (1)$$

Where T = temperature ($^{\circ}C$), K = thermal conductivity in x and y directions ($W/m^{\circ}C$), $\dot{q}$ = heat generation rate per

unit volume (j/s.m^3), C = material specific heat ($J/Kg\,°C$), ρ = material density (Kg/m^3) and t = time (s) [8].

3- The finite elements model

Application of the finite element method for solution of equation (1 (proceeds by dividing the problem domain into finite-length, two-dimensional rectangular elements and discretizing the temperature distribution within each element as:

$$T(x,y,t) = N_i(x,y)\,T_i(t) + N_j(x,y)\,T_j(t) + N_m(x,y)\,T_m(t) + N_n(x,y)\,T_n(t) = [N(x,y)]\,\{T(t)\} \quad (2)$$

Where $T_{i,j,m,n}$ are nodal temperatures, x and y axis of local (element based) coordinate system (the element coordinate system orientation is as described in figure2-(c)), t is the time and N_i, N_j, N_m, N_n are the nodal interpolation functions. The temperature distribution for a typical element in terms of shape functions is given by:

$$T^{(e)} = \begin{bmatrix} N_i & N_j & N_m & N_n \end{bmatrix} \begin{Bmatrix} T_i \\ T_j \\ T_m \\ T_n \end{Bmatrix} = \quad [N]\,\{T\} \qquad (3)$$

Where $[N]$ is the row matrix of interpolation functions and $\{T\}$ is the column matrix (vector) of nodal temperatures. The nodal temperatures are functions of time[9].

4. Numerical modelling

Applying Galerkin's finite element method to equation (1) to obtain the residual equations:

$$\int_A [N]^T \left(K_x \frac{\partial^2 T}{\partial x^2} + K_y \frac{\partial^2 T}{\partial y^2} + \dot{q} - C\rho \frac{\partial T}{\partial t} \right) dA = 0 \tag{4}$$

The residual equations can be rearranged and expressed as:

$$\int_A \left(C_1 \frac{\partial [N]^T}{\partial x} \frac{\partial T}{\partial x} \right) dA + \int_A \left(C_2 \frac{\partial [N]^T}{\partial y} \frac{\partial T}{\partial y} \right) dA + \int_A C_4 \frac{\partial T}{\partial t} [N]^T \, dA$$
$$= \int_A [N]^T C_3 \, dA + \int_A C_1 \frac{\partial}{\partial x} \left([N]^T \frac{\partial T}{\partial x} \right) dA + \int_A C_2 \frac{\partial}{\partial y} \left([N]^T \frac{\partial T}{\partial y} \right) dA \tag{5}$$

Where: $C_1 = K_x$; $C_2 = K_y$; $C_3 = \dot{q}$ and $C_4 = C\rho$ [9]. Utilizing equations (2) and (3), the integrals in equation (5) can be written in detailed matrix form as:

- Left hand terms

1st and 2nd integrals:

$\int_A C_1 \left(\frac{\partial [N]^T}{\partial x} \frac{\partial T}{\partial x} \right) dA$ and $\int_A C_2 \left(\frac{\partial [N]^T}{\partial y} \frac{\partial T}{\partial y} \right) dA$ gives

$[K_x] \begin{Bmatrix} T_i \\ T_j \\ T_m \\ T_n \end{Bmatrix}$ and $[K_y] \begin{Bmatrix} T_i \\ T_j \\ T_m \\ T_n \end{Bmatrix}$ respectively,

In which $[K_x]^e, [K_y]^e = \begin{bmatrix} K_{ii} & K_{ij} & K_{im} & K_{in} \\ K_{ji} & K_{jj} & K_{jm} & K_{jn} \\ K_{mi} & K_{mj} & K_{mm} & K_{mn} \\ K_{ni} & K_{nj} & K_{nm} & K_{nn} \end{bmatrix}_{Xy}$ are the element conductivity

matrices in x and y directions.

3rd integral:

$\int_A C_4 \frac{\partial T}{\partial t} [N]^T dA = [C] \begin{Bmatrix} \dot{T}_i \\ \dot{T}_j \\ \dot{T}_m \\ \dot{T}_n \end{Bmatrix}$ in which

$[C]^e = \begin{bmatrix} C_{ii} & C_{ij} & C_{im} & C_{im} \\ C_{ji} & C_{jj} & C_{jm} & C_{jn} \\ C_{mi} & C_{mj} & C_{mm} & C_{mn} \\ C_{ni} & C_{nj} & C_{nm} & C_{nn} \end{bmatrix}$ is the element

consistent capacity matrix.

- Right hand terms

1st integral:

$$\int_A [N]^T C_3 \, dA \qquad \left\{ f_Q^{(e)} \right\}$$

Is the element forcing vector due to internal heat generation using Green's Theorem, the 2nd and 3rd right terms in equation (5) can be written in terms of integrals around the element boundary (i.e. area integrals in terms of line integrals around the element boundary) as:

$$\int_A C_1 \frac{\partial}{\partial x}\left([N]^T \frac{\partial T}{\partial x} \right) dA = \int_\Omega C_1 \, [N]^T \frac{\partial T}{\partial x} \cos\theta \, d\Omega \tag{6}$$

$$\int_A C_2 \frac{\partial}{\partial y}\left([N]^T \frac{\partial T}{\partial y} \right) dA = \int_\Omega C_2 \, [N]^T \frac{\partial T}{\partial y} \sin\theta \, d\Omega \tag{7}$$

Where Ω represent the element boundary, and θ measure the angle to the unit normal. Equations (6) and (7) contribute to the derivative boundary conditions for conductance matrix $[K]^e$ and thermal load matrix $\{F_g^{(e)}\}$ [8, 9].

The derivatives of the interpolation functions have now been expressed as ordinary derivatives, as appropriate. Equation (5) is most often expressed as:

$$\left[C^{(e)}\right]\left\{\dot{T}^{(e)}\right\}+\left[K^{(e)}\right]\left\{T^{(e)}\right\}=\left\{f_Q^{(e)}\right\}+\left\{f_g^{(e)}\right\} \tag{8}$$

Where $\left[K^{(e)}\right]$ is the element conductance matrix, $\left\{f_Q^{(e)}\right\}$ element forcing vector due to internal heat generation, $\left\{f_g^{(e)}\right\}$ is element gradient vector due to boundary condition(s) and $\left[C^{(e)}\right]$ is the element capacitance matrix which was developed and as implied by its name, indicates the capacity of the element for heat storage.

The model assembly procedure for a transient heat transfer problem is that, element nodes are assigned to global nodes and the element capacitance matrix terms are added to the appropriate global positions in the global capacitance matrix, as with the conductance matrix terms[9]. Hence, on system assembly the global equations are:

$$[\mathbf{C}]\left\{\dot{\mathbf{T}}\right\}+[\mathbf{K}]\{\mathbf{T}\}=\{\mathbf{F_Q}\}+\{\mathbf{F_g}\} \tag{9}$$

5. Finite Difference Method

The finite element discretization procedure has reduced the two-dimensional transient heat transfer problem to algebraic terms in the spatial variable via the interpolation functions. A commonly used approach to obtaining solutions for ordinary differential equations of the form of equation (9) is the finite difference method. The finite difference method is based on approximating derivatives of a function as incremental changes in the value of the function corresponding to finite changes in the value of the independent variable. Applying the procedure to the transient heat transfer, the time derivative of the nodal temperature matrix in equation (9) is approximated using forward difference scheme (Euler's method) as:

$$[C]\{T(t_{i+1})\} = [C]\{T(t_i)\} - [K]\{T(t_i)\}\Delta t + \{F_Q(t)\}\Delta t + \{F_g(t)\}\Delta t \quad (10)$$

Where Δt is the time step. Note that, if the nodal temperatures are known at time t and the forcing functions are evaluated at time t, equation (10) can be solved, algebraically, for the nodal temperatures at time $t + \Delta t$ [9]. Denoting the time at the i^{th} time step as $t_i = i(\Delta t)$, $i = 0, 1, 2\ldots$ then gives:

$$\{T\}_{(i+1)} = \{T\}_{(i)} - [C]^{-1}[K]\{T\}_{(i)}\Delta t + [C]^{-1}\{F_g\}\Delta t \quad for\ i = 0,1,2,3,..... \tag{11}$$

Since there is no heat generation inside the system, the heat generation force vector term equal to zero $\{F_Q\} = 0$ .To begin the solution procedure the state of the system must be known at $t = 0$, in addition to applicable boundary conditions[9].

6. Material Properties of Sand Mould and Casting Alloy

Figure 1-(a) presents the geometry of the aluminum alloy part. The characteristics of sand and aluminum alloy are given in tables 1 and 2 [1]. It assumed that the physical properties for sand mould and aluminum alloy (liquid) are independent of temperature changes. The two-dimensional analysis of one unit thick slice was performed. Figure 1-(b) gives the geometry of the model. Half-symmetry was used to reduce the size of the model. The right half is the portion modeled figure 2-(a, b). Finite elements model consist of 72 2-D thermal solid elements, 48 for the sand mould and 24 for the alloy, with total number of nodes in the model of 91 figure 2-(a, b). The element has four nodes with a single degree of freedom (temperature) at each node. The

fixed mesh, rectangular bilinear finite element was used figure2-(c). It has equal length (L_e) and width (w_e) of (1cm). Boundary and initial conditions on the boundary of the model, excluding axis of symmetry, we supposed constant value for film coefficient (h_f = 11.443 w/m^2 ^{o}C) as well as air temperature (T_{air} =30^{o}C). In addition, we supposed uniformly distributed initial temperatures of sand (T_{sand} =30^{o}C) and alloy (T_{pour}=670^{o}C).

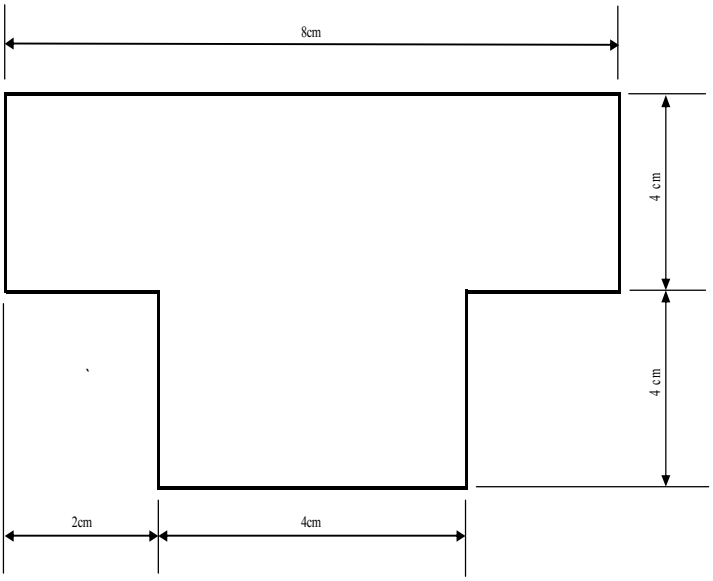

(a)

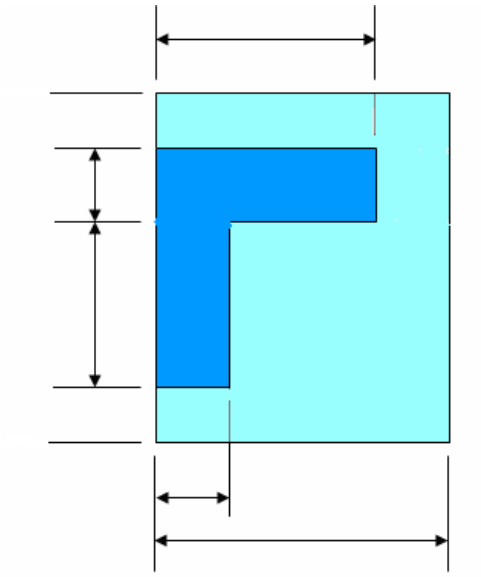

(b)

Figure 1: (a) Aluminum T-section part (b) Model geometry

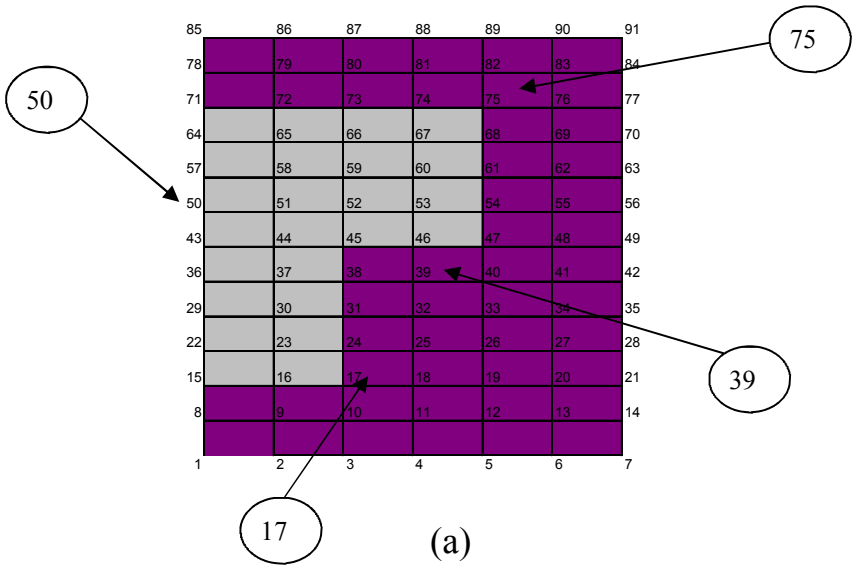

(a)

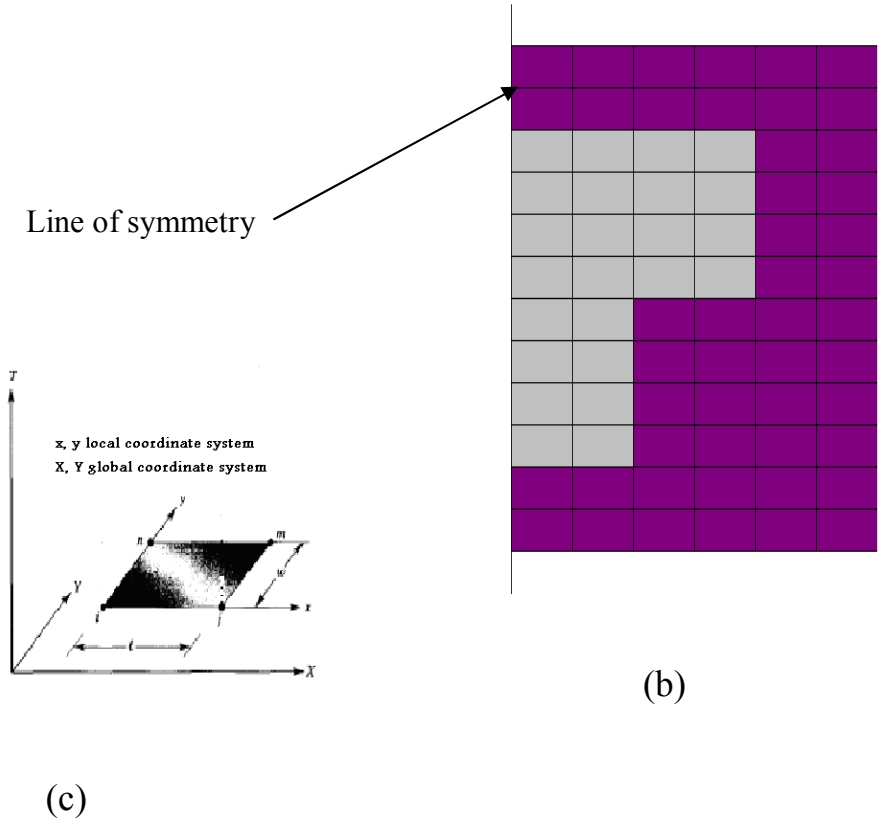

Figure 2: (a) Finite element model and position of observed nodes (b) Right hand half of model and line of symmetry (c) Geometry of one finite element

Table 1: Material properties of sand mould [1]

Physical quantity	value
Thermal conductivity	$K_1 = 1.5\ w/m°C$
Specific heat	$C_1 = 1117\ J/Kg°C$
Mass density	$\rho_1 = 1600\ Kg/m^3$
Film coefficient (sand-air)	$h_{sand-air} = 11.443\ w/m^2°C$
Initial temperature	$T_{init} = 30°C$

Table 2: Material properties of casting alloy [1]

Physical quantity	value
Thermal conductivity	$K_2 = 94.03\ w/m°C$
Specific heat	$C_2 = 1080\ J/Kg°C$
Mass density	$\rho_2 = 2385\ Kg/m^3$
Heat of fusion	$\Delta H_F = 395995\ J/Kg$
Pouring temperature	$T_p = 670°C$
liquidus temperature	$T_L = 640°C$
Solidus temperature	$T_s = 620°C$

The nonlinearity of the problem imposed subdivision of time domain on many subdomains. Therefore, time domain is sub divided into 0.1 divisions ($\Delta t = 0.1$ s). At the end of each time step, the nodal temperatures are calculated in order to obtain new equilibrium state. In order to avoid numerical instability (the growing of error while marching in time axis), the maximum time step size was controlled by the description of the loading input and the minimum time step size by defining its value based on the following relationship:

$$ITS = \Delta^2 / 4\alpha \qquad (12)$$

The ITS is the instability time step and Δ is the conducting length of an element along the direction of heat flow. The α value is the thermal diffusivity, given by $K/\rho C$. The K value is thermal conductivity, ρ is the mass density, and C is the specific heat[10,11]. If the above relationship is violated, unwanted numerical oscillations and values of calculated temperature outside of the physically possible range may occur[11]. The maximum time step size found is 0.5 second.

3. Results and discussion

The results of the simulation are shown in figures 3 to 9. The temperature distribution in the sand mould and alloy, after time intervals of t_1= 2.9s, t_2= 29.7s, t_3= 121.5s and t_4=4x10^4s are shown in figures 3-(a, b) and 4-(a, b) respectively. A family of temperatures history of the casting and mould configuration at intervals of 300 and 10^3 seconds are presented in figure 5-(a, b). The changes in temperature field distributions relate to model geometry with closer contours at the start than at the end of so-

lidification figure 3-(a, b). During the cooling period of 2.9s after pouring, 97.30% of casting nodes at temperatures above liquidus temperature (T_L) and alloy solidification process initially takes place at this moment at temperature level of (T_L = 640 $^{\circ}C$). The first point that solidifies lies at the top-right corner of the T-section flange shown as node N75 in figure 3- (a). The top - and bottom-right portions of mould represent the coldest zones. At the end of solidification (t_{end} = 29.7s), 97.3% of casting nodes at temperatures below its solidus temperature (T_s = 620 $^{\circ}C$). The last point solidifies lies at the left innermost above the intersection between the flange and the web of the T-section by 1cm (i.e. one quarter of flange depth) as shown in figure 3-(b) as node N50. The T-section takes about 26.8 seconds to solidify. While the casting was undergoing the cooling process, the mould heated and approached a maximum temperature of 424 $^{\circ}C$ at time of 121.5s from pouring figures 4-(a) and 5-(a). Node N39 is the location of maximum temperature in the mould and its temperature increased about 14 times from 30 to 424 $^{\circ}C$ figures 4-(a) and 5-(a). By the time the reminder of mould nodes are at a temperature between 346 and 31 $^{\circ}C$, while the casting temperature decreases to values between 514 and 495 $^{\circ}C$. Then after, the whole of system undergoes the cooling process until approaches the thermal equilibrium state at temperature level of (T_{air} = 30 $^{\circ}C$). The temperature history of the model before the equilibrium state at interval of 10^4 s and temperature distribution just before this state at $4x10^4$ s are illustrated in figures 5-(b) and 4-(b) respectively.

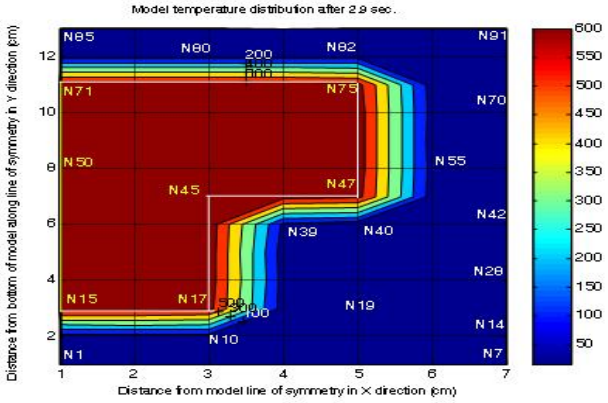

(a)

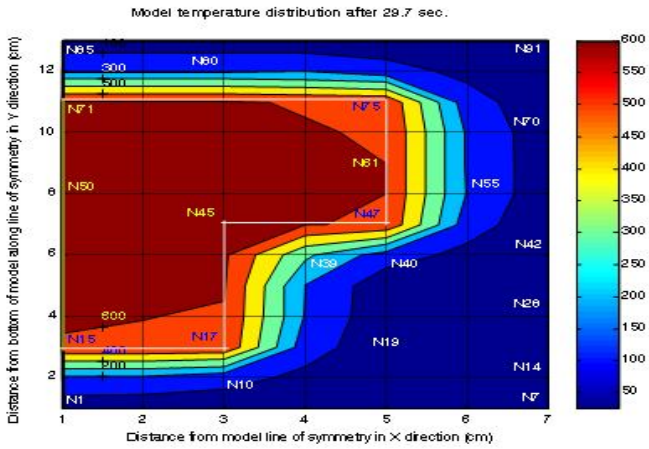

(b)

Figure 3: (a) Temperature field distribution [$^{\circ}C$] at the start of solidification (b) Temperature field distribution [$^{\circ}C$] at the end of solidification

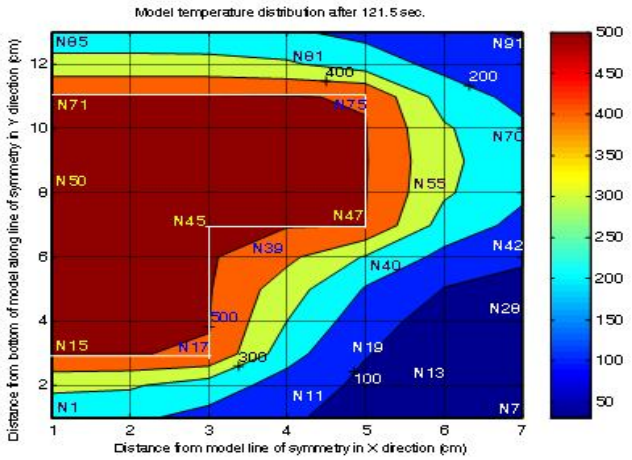

(a)

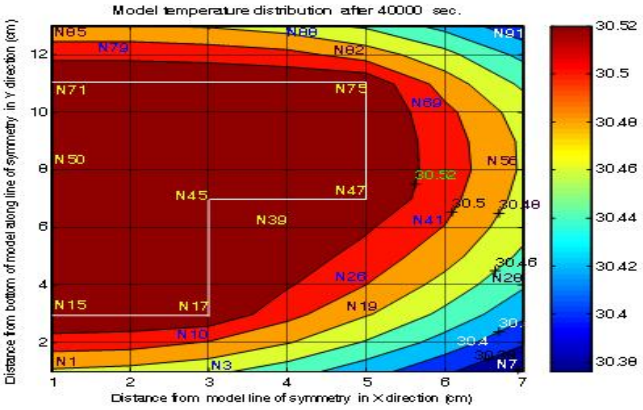

(b)

Figure 4: (a) Temperature field distribution [$^{\circ}C$] at mould peak temperature (b) Temperature field distribution [$^{\circ}C$] as model approach thermal equilibrium

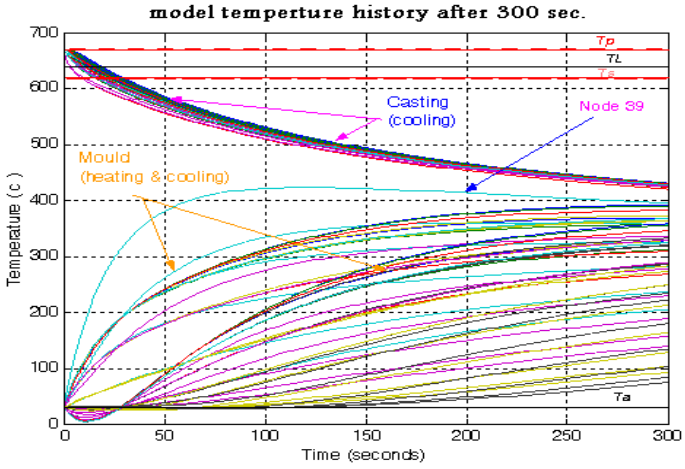

(a)

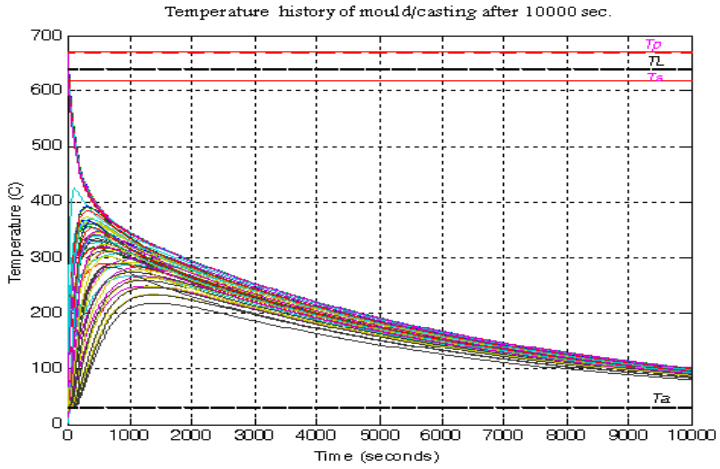

(b)

Figure 5: (a) Temperature history [$^{\circ}C$] after 300 sec. (b) Temperature history [$^{\circ}C$] after 10^4 sec.

The cooling and heating rates distributions in the casting and sand mould of model at start and end of solidification moments are illustrated in figures 6-(a, b). The distribution relates to model geometry. At start of solidification the top- and bottom-right corners of flange and the bottom-right corners of web nodes N75, N47and N17 have the highest value of 5 $^{\circ}C$ /s, because they are surrounded by more area of cold sand. The reminder of casting varies between 4 and 1 $^{\circ}C$ /s except node N50 undergoes no change. During this period the mould heated and node N39 has a higher value of 17 $^{\circ}C$ /s. The far away top- and bottom-right corners undertake no change. The remainder of mould heating rate varies between 10 to 1 $^{\circ}C$ /s. The distribution follows model geometry with narrower terrain towards the end of solidification. At this moment all casting nodes have a constant cooling rate of 2 $^{\circ}C$ /s except nodes N17, N47 and N75 of a value of 1 $^{\circ}C$ /s. While the mould heating rates drop down to values between 4 and 1 $^{\circ}C$ /s. The top- and bottom-right corners still undergo no change. The cooling rates history of nodes

N75 and N50 over a time period of 60s are presented in figure 7 -(a, b), where the solidification process starts and ends at these nodes respectively. In general the cooling rates are higher near the mould metal interface than the casting interior. Also the cooling rates are higher in the beginning and decreases as the solidification progresses.

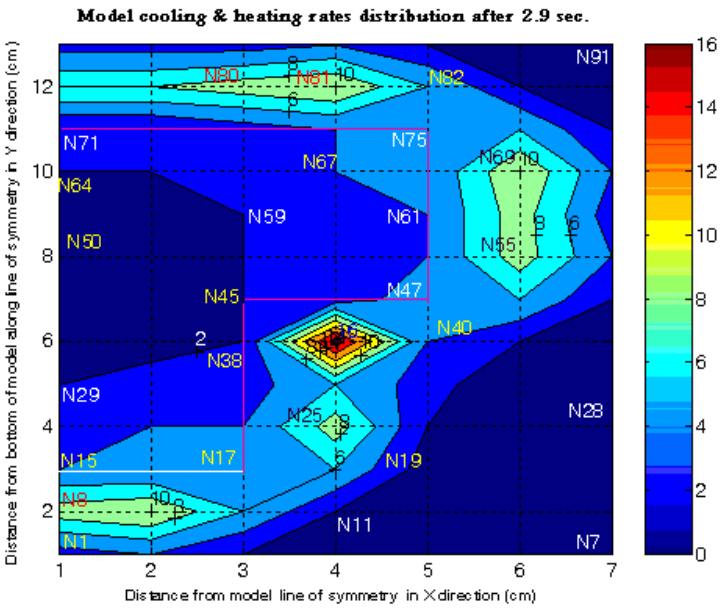

(a)

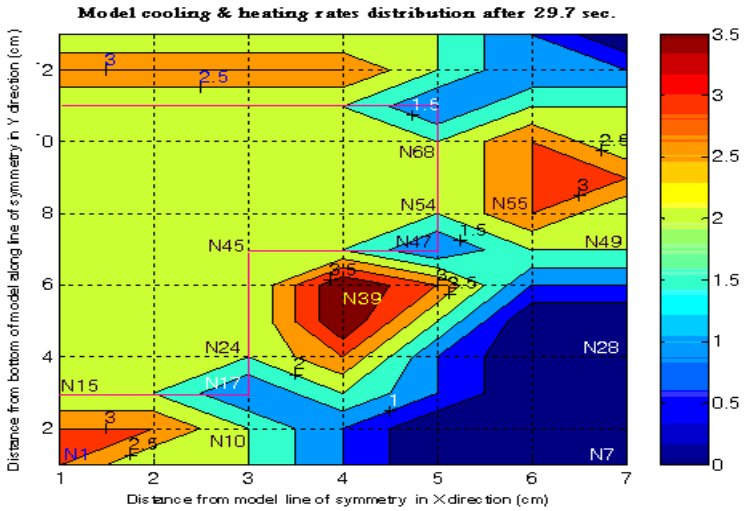

(b)

Figure 6: (a) Cooling and heating rate distribution [$^{\circ}C$ /s] at start of solidification (b) Cooling and heating rate distribution [$^{\circ}C$ /s] at end of solidification

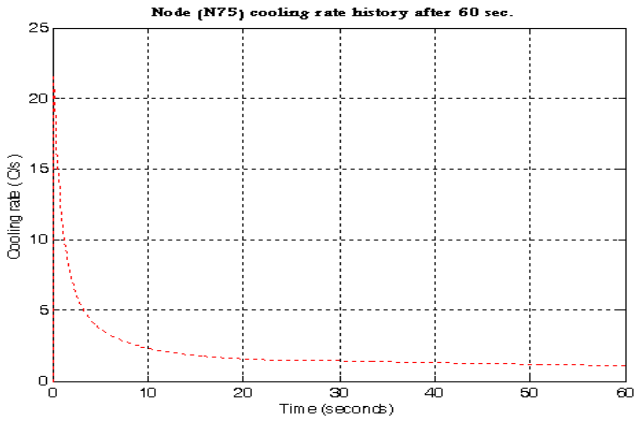

(a)

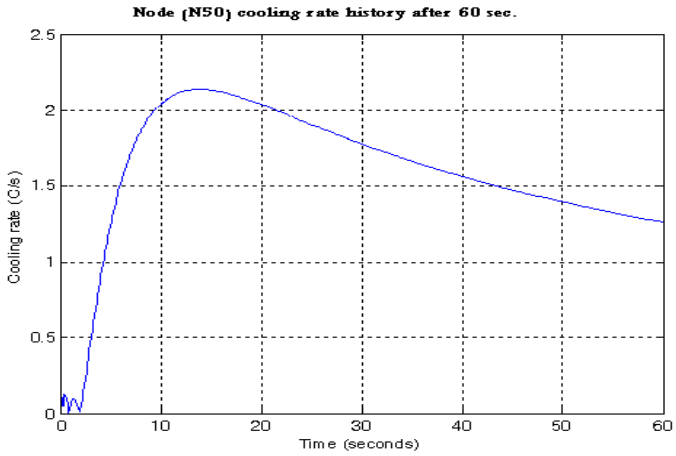

(b)

Figure 7: (a) Node (N75) cooling rate history [$^{\circ}C$ /s] after 60 sec. (b) Node (N50) cooling rate history [$^{\circ}C$ /s] after 60 sec.

The thermal gradient distributions in the casting and sand mould of model at the start and end of solidification intervals are shown in figure 8-(a, b). The distributions relate to model geometry with wide terrain. At start of solidification the bottom-right corner of the web N17 has the highest value of 205K/mm. The reminder of casting varies between 204 to 1K/mm. During this period the mould heated and node N39 of a high value of 193K/mm. The rest of mould varies between 133 and 1K/mm. The top- and bottom-right regions of the mould with zero gradi-

ents that are thermally balanced. The thermal gradient distribution in the mould and casting at the end of solidification relate to model geometry with wider terrain. At this moment the casting gradient drops as the time proceeds to values between 151 to 1K/mm, however the gradients nodes N43 and N50 their gradients increase from zero to 1K/mm. The mould gradient drops down to values between 69 to 1K/mm, excepting its farthest bottom-right portion still have zero gradients that are in thermal equilibrium. The thermal gradients history of nodes N75 and N50 over time period of 60s is presented in figure 9-(a, b), where the solidification process starts and ends at them respectively. Generally the thermal gradients of casting at the locations near mould wall are characterized by high gradients, whereas the middle regions of casting have low gradients. Also the gradients are higher in the beginning and decreases as the solidification proceeds.

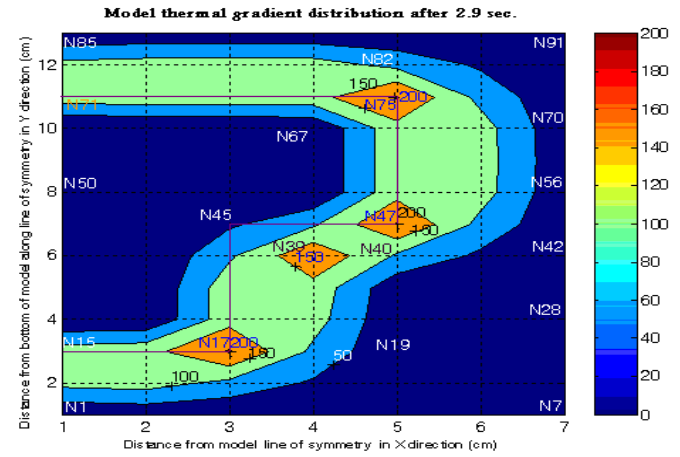

(a)

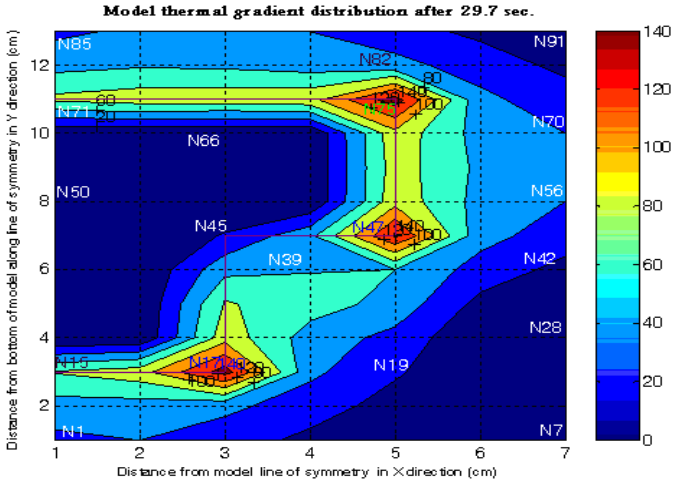

(b)

Figure 8: (a) Thermal gradient distribution [K/mm] at the start of solidification (b) Thermal gradient distribution [K/mm] at the end of solidification

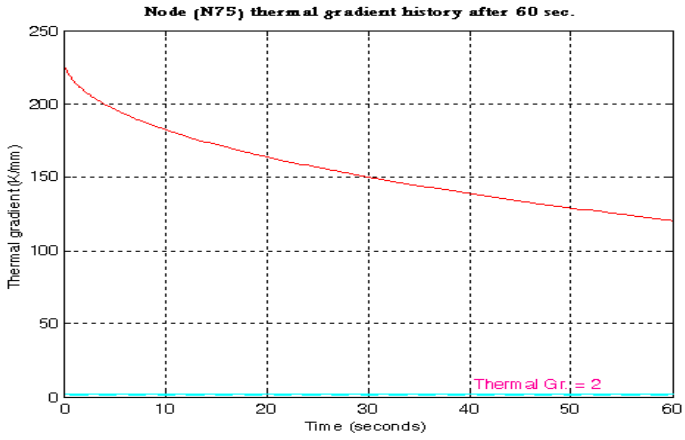

(a)

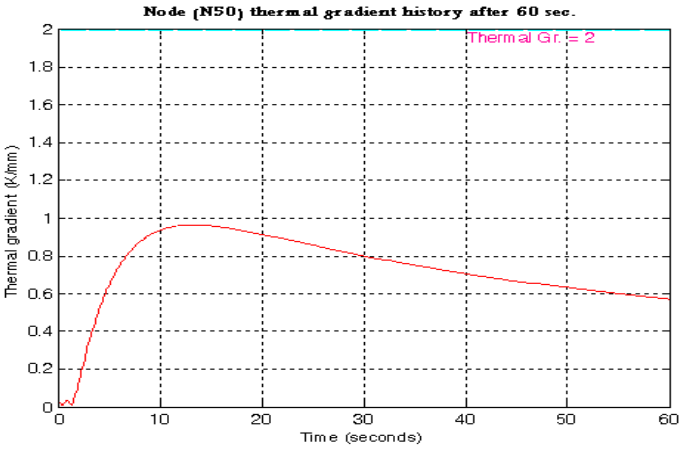

(b)

Figure 9: (a) Node (N75) thermal gradient [K/mm] after 60 sec. (b) Node (N50) thermal gradient [K/mm] after 60 sec.

It is obvious that the conducted work is an attempt to bring the foundry practice to a more scientific basis towards virtual foundry and to integrate the design process concurrently with heat transfer. Moreover, the simulation results can be manipulated in many ways to track other related phenomena. The current work provides variety of mapping systems that aids in inferring valuable information used by different interested in and aware of relevant fields. The following comments were deducted on the model performance:

- The model demonstrates plainly the phenomenon of progressive and directional solidification that casting prevails. The mould material stimulates the insulating effect and reduces the rate at which heat is extracted. This reflects that the retained heat in casting is exchanges to raise the temperature of the mould. During the solidification phase the general profile of the cooling rate decreases and the thermal gradient increases as the time proceeds.
- When the depth of web is one half the breadth of flange and the modulus of flange is greater than of the web, the last region solidified lies inside the largest inscribed circle of the T-

section and above their intersection along the line of symmetry by one quarter of the flange depth figure 3-(b). This result commensurate with Chvornov's rule and precisely identify the position of the last freezing region (hot spot) in contrast to this rule, which roughly indicate this region.

- The thermal gradients of the last freezing region in the model is always less than the minimum critical value for alloy (G_C = 2K/mm), figure 9-(b), This outcome rigorously confirms with thermal gradient rule, that when its value falls at any time below a critical minimum value $\left(\frac{dT}{dX}\right)_C$, shrinkage voids are were most likely formed[4].

- Observing the last freezing location in the model, it is characterized by high temperature, low gradient and high cooling rate relative to its adjacent regions, specifically towards the end of solidification. This finding strictly matching the rule that suggest the location of shrinkage defects, are of high temperature, coupled with low gradient and high cooling rate.

7. Conclusion

This model enables, taking into account all assumption imposed, an insight to be gained into details of temperature, cooling rate and temperature gradient changes during aluminum alloy solidification and the complete cycle of heat flow process in the model. In addition, quantitative determination of these properties is available with logical perspective behaviors of the system. According to the results of the analysis, the start and end of solidification locations are geometrical driven. Geometry of sand mould has an important impact on heat transfer process through material, as well as on temperature, cooling rate and temperature gradient distribution in the model. So, additional analysis of mould geometry influences on the solidification of aluminum alloy, with all related boundary and initial condition taken into account, is necessary to conduct in order to define the type and level of these influences.

The result obtained could be also used for further coupled thermal structural analysis in order to investigate the occurrence of other casting defects. In addition, new transient heat transfer analysis of this model with new, forced cooling condition should

be conducted in order to determine the best cooling condition regarding the appearance of this residual stresses.

References

[1] Karl B. Rundman, "Metal casting", 1st edition , Michigan Tech. University, 2005.

[2] AFS, "Sources of Casting Modeling Software", Modern Casting, Vol.87, No. 10, 1997, pp. 27-29.

[3] B. Ravi and M. N. Srinivasant, "Casting Solidification Analysis by Modulus Vector Method", Int. J. Cast metals Res., 1996.

[4] B. RAVI, "Metal Casting: Computer-Aided Design and Analysis", 1st edition, Prentice-Hall of India, New Delhi, 2005.

[5] R. L. Lewis, S. Liou and Y. D. Shin, "Literature Review of Solidification Simulation in the Design of Sand Casting", Steel founders' Research Journal, 1987,17, pp. 1-1.

[6] T. X. Hou, R. D. Pehlke and J. O. Wilkes, "FEM Simulator for Efficient Casting Solidification Modeling", AFS Transactions, 1992, v100, pp. 1057-1066.

[7] L. Estrin, "Adeeper Look at Casting Solidification Software", Modern casting, 1994, V84, pp. 20-23.

[8] Saeed Moaveni, "Finite Element Analysis: Theory and Application with ANSYS", Prentice Hall, New Jersey, 1999.

[9] David V. Hutton, "Fundamentals of Finite Element Analysis", 1st edition, McGraw-Hill Companies, 2004.

[10] Roland W. Lewis et al, "Fundamentals of the Finite Element Method for Heat and Fluid Flow", John Wiley & Sons, England, 2004.

[11] ANSYS Documentation, release 9.0, SAS IP In, 2008, pp.14-19.